Article

Catalytic Effect of Reactive Extraneous Mineral Composites on Char and Tar Distribution during Pyrolysis of Highveld Partially Oxidized Fine-Coal Reject and Its Beneficiated Residues

Katlego Mphahlele,* Ratale Henry Matjie, and John Reginald Bunt

Cite This: ACS Omega 2023, 8, 36479−36492

Read Online

ACCESS | Metrics & More | Article Recommendations

ABSTRACT: In this study, the South African partially oxidized fine-coal reject (FCR), which is associated with human health and environmental problems and sustains high disposal expenses, was subjected to density-separation, chemical fractionation, and demineralization experiments to isolate and evaluate the mode of occurrence of mineral-matter (MM) effects on the FCR pyrolysis. A unique composite of two reactive oxides (i.e., MgO and Fe_2O_3) and a hydrated oxide [i.e., $Ca(OH)_2$] representing major extraneous coal−minerals were blended with either FCR, demineralized FCR, and its beneficiated samples to evaluate the yields of pyrolytic products and activation energy following a novel procedure. The properties of FCR samples and their pyrolytic products were determined by different analyses. Results indicate that the reactive oxides and a hydrated oxide composite addition increased the average activation energy (332.0−476.5 kJ/mol) for FCR due to the initial $Ca(OH)_2$ decomposition and Fe_2O_3 reduction that took place under pyrolysis conditions. The FCR mineral-rich sink fractions achieved the highest carbon conversion (char yield = 78.8% and tar yield = 5.1%) compared to those of other samples (e.g., <1.9 g/cm^3 float char yield = 87.3% and tar yield = 2.3%) evaluated due to higher proportions of calcite/dolomite/pyrite cleats and nonmineral inorganics (Ca, Mg, Na, and Fe) which catalyzed the pyrolysis reactions. On the other hand, $CaCO_3$, $CaMg(CO_3)_2$, and metakaolinite formations in the char derived from a blend of reactive oxides and a hydrated oxide composite and FCR interfere with the pyrolysis reactions. Also, deoxygenation reactions were impeded by oxygen present in the reactive oxides and a hydrated oxide composite. The potent catalytic effects of cleat minerals and the extraneous minerals associated with cracking of heavy tars to lighter fractions open opportunities to further understand the mode of occurrence of MM present in FCR during utilization in global pyrolysis. This may reduce waste disposal costs, health-hazards, air-pollution, and FCR volumes and augments feed-coals.
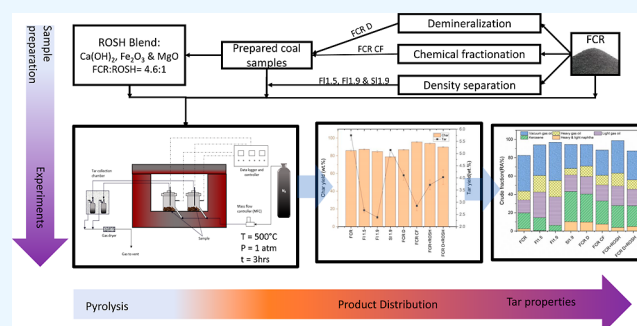
1. INTRODUCTION

Mechanized mining, handling, and processing of South African (SA) run-of-mine (ROM) coals, raw coals which are extracted and transported directly from the collieries, produce more than 60 million tonnes of partially oxidized fine-coal rejects (FCRs) annually, which are unsuitable for utilization in some thermochemical processes due to their fine nature.[1−4] As a result, about 1 billion tonnes of FCRs containing sulfur-bearing mineral-matter (MM) (>1%) have been disposed of in slurry ponds and stockpiles in the country. These FCRs contain ultrafine particles (<250 μm) and coarser fine-coal particles (250−1000 μm) which are amenable to spontaneous combustion resulting in SO_2, particulate matter (PM), nitrogen oxides (NOx), and CO_2 gas emissions during storage in stockpiles and slime dams.[1−4] This literature[1−4] reports that FCRs have chemical properties similar to coals utilized in boilers and gasifiers (i.e., feed-coals) but are classified as high-ash coals. The term "high-ash coals" refers to coals which are

produced from SA collieries comprising a percentage ash yield (AY) greater than 30%. The similar chemical properties indicate a potential to utilize FCRs as a cofeed to thermochemical processes such as pyrolysis, gasification, and combustion without following the current waste disposal methods which are associated with higher costs and health and environmental risks.

The SO_2 and NOx emissions associated with spontaneous combustion of FCR during storage are linked to the inflammation and irritation of the skin and respiratory system while CO_2 is responsible for global warming.[5] Additionally, the

inhalation of PM generated from conventional FCR storage causes chronic lung diseases (pneumoconiosis and tuberculosis) and silicosis (bronchitis symptoms and asthma).[6] Chalcophile elements such as As, Se, Cd, Ni, and Pd are associated with sulfide minerals present in coal.[7] These elements have been linked with carcinogenic and mutation effects.[7] The propensity for release of these toxic elements depends on their mode of occurrence which contributes to their transformation during pyrolysis and gasification processing.[8] According to Pone et al.,[9] spontaneous combustion of SA coals releases toluene, benzene, xylene, bromomethane, iodomethane, trichloromethane, dichloromethane, chloromethane, methane, CO_2, CO, Hg, As, Pb, Zn, and Cu into the atmosphere. Benzene, toluene, and xylenes are associated with carcinogenic proprieties.

However, like feed-coal, FCR which is generated during the preparation of Highveld feed-coals comprises various types of MM such as extraneous minerals (EM) (i.e., discrete mineral particles) and inherent MM (i.e., submicron mineral cleats and nonmineral inorganics), and macerals of vitrinite, inertinite and liptinite groups, all of which undergo a chemical transformation during thermochemical treatment of coal.[4,10,11] For instance, either extraneous fluxing minerals (i.e., dolomite, calcite, and pyrite) or inherent fluxing minerals which are associated with either extraneous or inherent kaolinite in the coals react to each other at elevated temperatures (>900 °C) to form the molten solution.[11,12] The heated rock fragments (mudstone, sandstone, and siltstone) present in the coals are attached to the molten solution to form lump heterogeneous clinkers in the commercial gasifiers or commercial boilers. The slow cooling of the molten material at lower temperatures (<340 °C) in the commercial gasifier-bed, mullite ($Al_6Si_2O_{13}$), and anorthite ($CaAl_2Si_2O_8$) crystals and Ca/Fe/Mg-bearing aluminosilicate glasses are formed. These heterogeneous clinkers with hard minerals (quartz and anorthite) cause deposition, blockage, and erosion problems and encapsulation of fine carbon particles, consequently lowering carbon conversion efficiencies during thermochemical processes.[11]

Pyrolysis is a useful technique for studying the reaction mechanisms involving the interaction of MM and the carbon matrix (macerals) to form precursors (i.e., tar, char, and gas) during thermochemical processes. These reaction mechanisms form tars and gases drying, via devotilization, primary decomposition, secondary cracking, catalytic cracking, and isomerization pathways, and char via carbonization reactions.

Several researchers performed pyrolysis experiments to evaluate the catalytic effects of inherent and EMs of Chinese, Japanese, American, and Middle Eastern coals.[13–15] Fu et al.[13] studied and compared the individual reactivity effects of potassium chloride (KCl), CaO, and Fe_2O_3 during pyrolysis of North Chinese low-rank coal and reported the catalytic potency in the order of Fe_2O_3 > KCl > CaO. The three minerals resulted in three different reaction effects: KCl promoted the tar yield, CaO promoted the gas yield, and Fe_2O_3 promoted the char yield. The results indicated that K (ion-exchangeable), CaO, and Fe_2O_3 mixing reduced the bond energy of oxygenated functional groups and enhanced the pyrolysis reactions.

He et al.[14] used ion-exchangeable Na, Ca, and Mg as individual and binary mixtures with Fe to study their catalytic effects and synergies with Fe on demineralized and raw coals. Their results indicated a catalytic activity by Na, Ca, K, and Mg due to the combination of these alkali and alkaline earth metals (AAEM) with the oxygenated functional groups, which facilitated the interaction of char and Fe. Furthermore, understanding the behavior of mode of occurrence of coal MM is minimized by acid washing, and as a result, it is not well discerned during pyrolysis.

Understanding the behavior of inherent and EMs as well as nonmineral inorganics in waste coal materials such as FCR could allow process operators/decision makers to take advantage of coal MM properties to improve process efficiencies instead of using specialized catalysts. To the authors' best knowledge, there are limited reports on the effects of ternary reactive mineral composites representing inherent or derivatives of inherent coal cleat minerals and nonmineral inorganics in partially oxidized coal fine waste on product distribution during pyrolysis of this FCR.

Therefore, an in-depth understanding of the catalytic effects of Ca, Mg, and Fe associated with the mode of occurrence of the MM in FCR under thermochemical processing conditions is a necessity for efficient and environmentally feasible co-utilization of these partially oxidized coal-fine wastes in global thermochemical processes. As a result, this study aims to close the gap by evaluating the effects of the mode of occurrence of coal MM in the FCR on the distribution and composition of pyrolytic products. The interaction of inherent and extraneous coal MM with an extraneous model composite of two commercial reactive oxides (MgO and Fe_2O_3) and hydroxide [$Ca(OH)_2$] (ROSH) present in EMs with an extension to their catalytic or hindrance effects were evaluated during the pyrolysis of FCR samples.

Generally, catalysts have been applied widely in chemical production to lower operating temperatures and pressures and to facilitate product selectivity.[15] In this study, the selected ROSH only served to simulate EMs with catalytic effects to understand their nature and behavior during the FCR pyrolysis. Furthermore, the addition of ROSH composites which are not co-feedstock of this proposed pyrolysis to the FCR samples may possess novel insights and perspectives that can considerably enhance better understanding of the mode of occurrence of EMs on char and tar yields during the FCR pyrolysis. Density separation, demineralization, and chemical fractionation procedures served only as techniques (they are not steps of the proposed low temperature pyrolysis) to isolate different modes of occurrences of MM and carbon matrices of FCR and to discern their effects in pyrolysis reactions. The Fischer assay experiments, mineralogical [X-ray diffraction (XRD)] and chemical [proximate, ultimate, X-ray fluorescence (XRF), Brunauer, Emmett, and Teller (BET) surface area, and gas chromatography−mass spectrometry (GC/MS)] analyses, along with activation energy analysis, were adopted to achieve the objectives of this novel study.

2. MATERIALS AND METHODS

2.1. FCR Sampling and Preparation. The FCR sample used in this study was collected from the SA thermal-export plant (TEP) disposal site, which is situated in the Highveld coalfields of the Mpumalanga Province of South Africa. A representative sample (250 kg) of the SA Highveld FCR was taken following the guidelines illustrated by the International Organization for Standardization (ISO), ISO 18283, and ISO 13909-4 standard methods for treatment, characterization, and experiments.

2.2. Density Separation. A representative portion of the sample (25 kg) was submitted to the General Society of
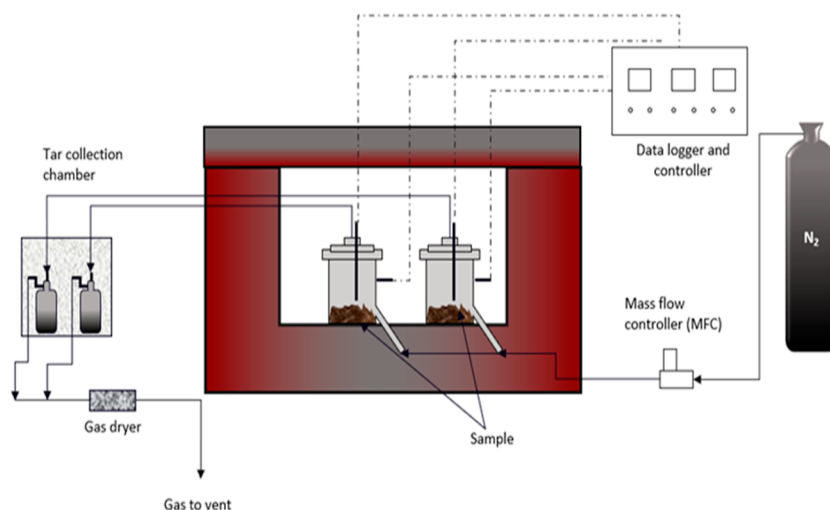
Figure 1. Schematic of the modified Fischer assay experimental rig used to conduct the pyrolysis experiments. Adapted with permission from Roets et al.[18] Copyright 2014, Elsevier.

Surveillance (SGS) Laboratories (PTY) Ltd., South Africa for the density separation procedure to produce three density-separated fractions (Fl 1.5 = <1.5 g/cm³ float; Fl 1.9 = <1.9 g/cm³ float; and Sl 1.9 = >1.9 g/cm³ sink) for this investigation following procedures described in the ISO 7936 standard method. Mixtures of tetrabromoethane, benzene, and tetrachloroethylene, with respective densities of 2.95, 0.879, and 1.62 g/cm³, were used to produce 1.5 and 1.9 g/cm³ floats and sink media, as indicated by Rautenbach et al.[4]

2.3. Demineralization Experiments. A three-step demineralization approach[16] using 10 mol/dm³ (M) hydrochloric acid (HCl) (37%, Sigma-Aldrich) and 22 M hydrofluoric acid (HF) (45%, Minema Chemicals) was followed for 24 h to dissolve almost all of MM from the FCR sample. The acid-treated sample without EMs and low proportions of inherent MMs was labeled FCR D for experiments and analyses.

2.4. Chemical Fractionation Procedure. The chemical fractionation procedure[17] was employed to leach nonmineral inorganics in FCR. The leached FCR labeled FCR CF and the leachate samples were submitted for XRD, XRF, and ICP analyses, respectively. The FCR CF was evaluated in the pyrolysis experiments to investigate the catalytic effect of the mode of occurrence of MM during pyrolysis.

2.5. Preparation of Blends of Coal and ROSH Composites. The ROSH [i.e., Fe_2O_3, MgO, and $Ca(OH)_2$] (98, 99, and 70%, respectively, CC Imelmann cc) composite made up of reactive oxides and hydrated oxide minerals of EMs typically present in SA feed-coals was prepared by combining these oxides and hydroxide of EMs at a mass ratio of 1:0.7:1 to increase proportions of reactive oxides and hydrated oxide minerals and Ca, Mg, and Fe in these blends for the unique pyrolysis experiments. The composite was mixed with either FCR or FCR D separately to prepare two (2) blends with 18 wt % ROSH and 82 wt % of either FCR sample or FCR D. This ratio was chosen to ensure the saturation of MM content in FCR D and FCR samples. Each blend was ground for 5 min in a rod mill to prepare a homogenized coal sample and ROSH blend sample with improved particle-to-particle contact. Before experiments and characterization, the homogenized samples were stored in an airtight container under nitrogen and labeled FCR + ROSH and FCR D + ROSH.

2.6. Pyrolysis Experiments. The pyrolysis experiments were carried out at an average internal temperature of 500 °C and an internal heating rate of 5 °C/min using the double retort Fischer assay rig, as reported by Roets et al.,[18] whose schematic diagram is presented in Figure 1.

A previous study by Roets et al.[18] indicated that both char and tar yields for Highveld feed-coal, as well as its density-separated fractions, decrease as the final pyrolysis temperatures increase from 450 to 900 °C.[18] On the other hand, Liu et al.[19] reported that the maximum tar yield was produced at 600 °C. Considering the insights from these two studies and the fact that the initial transformation and decomposition of coal minerals and macerals commence at temperatures above 450 °C under oxidizing and nitrogen conditions, a temperature of 500 °C and time of 3 h were selected for the current study.

About 45 ± 0 5 g of sample was placed in a retort, allowing a 3 cm freeboard area. The retort was tightened with bolts, to which copper grease was applied, and was carefully placed in the oven. In the initial stage of the experiments, nitrogen baseline 5.0 [99.995%, AFROX (PTY) Ltd.] flowing at 2 NL/h was used to purge oxygen and create an inert atmosphere. After 10 min, the flow of N_2 was stopped, and heating was initiated. The volatiles that evolved during the process were bubbled through a toluene (99%, CC Imelmann cc) tar trap, and a gas washing system submerged in an ice bath. The gases produced were vented and not captured. The gas−liquid (condensate) fraction was separated from the tar and toluene mixture using a Dean−Stark distillation setup. The cooled tar−toluene mixture was subjected to vacuum distillation using a Buchi R100 rotor vapor setup equipped with a Buchi V100 vacuum pump at 55 °C and 75 mbar until no visible condensation of toluene was observed in the collection flask. The tar, gas-liquor, and char yields were determined based on their weights and corrected using eqs 1−4. The gas yields were determined by difference, according to the ISO 647 method. The pyrolysis product distribution of the various fractions (char, tar, gas, and water) was evaluated based on their weight. It was important to present the yields on an ash-free basis to correct for the contribution of MM to char and gas-liquor yields.

Table 1. Proximate and Ultimate Results for FCR, Beneficiated Fractions, Acid-Washed Residues, and ROSH Blends along with Their Corresponding Chars[a]

parameter	proximate results (wt % adb)				ultimate results (wt % daf)				
	IM	AY	VM	FC[a]	C	H	N	O[a]	TS
FCR	4.2	28.7	22.0	45.1	78.7	4.5	1.9	13.7	1.2
FCR[C]	1.1	33.3	13.5	52.2	84.8	3.2	2.3	8.7	1.1
FCR + ROSH	3.7	40.6	22.1	33.6	76.3	4.7	2.0	16.0	1.1
FCR + ROSH[C]	1.0	44.8	15.3	38.9	85.2	3.0	2.0	8.7	1.1
Fl 1.5	5.8	19.0	28.8	46.4	74.8	4.5	1.9	17.8	1.1
Fl 1.5[C]	3.7	23.2	13.8	59.3	83.6	3.1	2.2	10.4	0.7
Fl 1.9	7.0	26.2	24.0	42.8	74.1	4.0	1.9	18.7	1.2
Fl 1.9[C]	4.5	30.3	14.3	50.9	83.0	3.1	2.0	11.0	0.9
Sl 1.9	7.6	31.9	23.8	36.7	72.3	3.6	1.8	20.9	1.3
Sl 1.9[C]	4.4	32.3	14.3	49.0	83.3	3.2	2.1	10.6	0.9
FCR D	3.3	1.3	28.8	66.6	78.7	4.4	2.1	13.6	1.2
FCR D[C]	2.0	1.8	13.2	83.1	86.5	3.0	2.3	7.5	0.7
FCR D + ROSH	3.5	20.1	26.2	50.2	80.8	4.6	2.1	11.6	0.9
FCR D + ROSH[C]	1.7	22.5	14.6	61.3	86.8	2.8	2.2	7.2	0.9
FCR CF	2.8	24.8	23.5	48.9	77.6	4.6	2.2	14.5	1.1
FCR CF[C]	1.6	15.1	13.2	70.1	87.8	3.2	2.3	5.9	0.8

[a]Daf—dry ash-free basis, adb—air-dried basis, IM—inherent moisture, AY—ash yield, VM—volatile matter, FC—fixed carbon, TS—total sulfur, "a"—determined by difference, and "C"—char.

$$Y_{char} = \frac{M_{char} \times (1 - A_{char})}{M_{sample} \times (1 - A_{sample})} \times 100\% \tag{1}$$

$$Y_{tar} = \frac{M_{tar}}{M_{sample} \times (1 - A_{sample})} \times 100\% \tag{2}$$

$$Y_{gasliquor} = \frac{M_{gasliqour}}{M_{sample} \times (1 - A_{sample})} \times 100\% \tag{3}$$

$$Y_{gas} = 100\% - Y_{char} - Y_{tar} \tag{4}$$

whereby "Y" refers to yields of either char, tar, gas-liquor, or gas in percentage, "A" refers to the dimensionless fraction of AYs for char and sample, and "M" to the mass of either sample, char, tar, or gas-liquor in grams.

After the initial calculations, the values were normalized on a gas-liquor free basis. To minimize noise and the effects of uncontrolled variables, the samples were rotated between the retorts for all repeated experiments. The experiments were repeated at least 3 times with a 5% experimental error. The weighted averages of these samples were considered.

2.7. Proximate, Calorific Value, Ultimate, XRF, XRD, BET Surface Area, GC/MS, and Activation Energy Analyses. The pulverized FCR, its beneficiated samples, FCR D + ROSH and FCR + ROSH blends, and their corresponding chars (<75 μm) were submitted at the Laboratories of Bureau Veritas Testing and Inspections South Africa (Pty) Ltd. for proximate, ultimate, and sulfur analyses distribution using the standard coal analyses,[4] respectively.

The XRF analysis (ASTM D4326-13)[20] was followed to determine the proportions of inorganic elements contained in the ashes of the FCR, FCR D, FCR CF, Fl 1.5, F 1.9, and SI 1.9 samples and FCR D + ROSH and FCR + ROSH together with their corresponding chars.

The same pulverized samples above together with their prepared blends and their chars (<75 μm) were analyzed by

the XRD using mineralogical methods which are developed and described by Speakman[21] and Rietveld.[22]

The BET surface area analysis[23] of either prepared coal samples or their corresponding char samples were performed using the North-West University (NWU) Micrometrics ASAP 2020 BET instrument.

The NWU Agilent 7890 GC-MSD GC coupled with a 5975 Triple Axis MSD detector was used to elute, detect, and identify chemical components in the pyrolytic tars.[16]

The thermogravimetric analyzer (SDT Q600 TGA) at NWU was used to perform analytical pyrolysis of FCR, FCR CF, FCR D, FCR D + ROSH, and FCR + ROSH samples at three heating rates (i.e., 10, 15, and 20 °C/min). A detailed description of the activation energy analysis technique can be found elsewhere.[24,25] Equation 5 is the simplified Starink[25] technique derived from the Arrhenius equation.

$$\ln\left[\frac{\beta}{T_x^{1.8}}\right] = C - 1.0037\left[\frac{E_a}{RT_x}\right] \tag{5}$$

whereby β is the heating rate, C is the constant or x intercept, E_a is the apparent activation energy, R is the universal gas constant, and T_x is the temperature at conversion x. A linear plot of $\ln\left[\frac{\beta}{T_x^{1.8}}\right]$ versus (vs) $\frac{1}{T}$ with $-1.0037\left[\frac{E_a}{R}\right]$ as the gradient is obtained from analytical data to estimate the E_a values.

3. RESULTS AND DISCUSSION

3.1. Coal and Char Compositions. Proximate results of the FCR, its beneficiated samples, FCR D + ROSH and FCR + ROSH blends, and their corresponding chars are reported on an air-dried basis (Table 1). As expected, these results indicate a decrease in the AY % for the FCR D and FCR CF samples. Over 95 wt % of MM removal was achieved by the demineralization experiments, which changed the overall coal structure of FCR. On the other hand, the chemical fractionation procedure achieved only 13 wt % MM removal in FCR. These MM removal efficiencies are consistent with those of SA Highveld coals which are reported by Raghoo.[17]

Table 2. Chemical Composition for FCR, Beneficiated Fractions, Acid-Washed Residues, and ROSH Blends along with Their Corresponding Chars[a]

element (LOI free wt %)	SiO$_2$	Al$_2$O$_3$	CaO	Fe$_2$O$_3$	MgO	TiO$_2$	K$_2$O	Na$_2$O	P$_2$O$_5$	SO$_3$
FCR	52.0	23.7	9.8	3.5	2.1	1.5	1.0	0.7	0.7	4.4
FCR[C]	49.0	25.9	8.0	5.9	2.5	1.4	1.0	0.6	0.6	4.1
FCR + ROSH	31.6	16.1	15.1	15.9	14.4	0.9	0.7	0.4	0.4	3.9
FCR + ROSH[C]	32.1	16.7	15.3	16.0	13.4	0.9	0.7	0.4	0.4	3.6
Fl 1.5	48.6	28.5	6.9	4.2	2.0	1.6	1.1	0.9	0.9	4.3
Fl 1.5[C]	47.0	28.0	6.9	6.8	2.0	1.6	1.0	0.7	0.9	4.1
Fl 1.9	50.2	27.6	7.3	3.9	2.0	1.4	1.1	0.8	0.7	4.1
Fl 1.9[C]	49.6	27.8	7.2	5.8	1.9	1.4	1.0	0.7	0.7	2.9
Sl 1.9	51.2	25.2	8.2	4.8	1.9	1.3	1.1	0.6	0.5	4.3
Sl 1.9[C]	50.1	27.3	7.4	6.7	2.1	1.4	1.1	0.7	0.6	1.7
FCR D	6.3	10.1	6.2	50.4	1.6	10.0	0.1	5.0	0.4	9.9
FCR D + ROSH	4.6	1.3	23.2	31.6	29.3	0.6	0.0	0.1	0.1	8.6
FCR D + ROSH[C]	5.1	1.6	22.9	32.7	28.1	0.6	0.0	dl	0.1	8.3
FCR CF	58.6	31.9	0.4	4.1	0.4	1.7	1.2	0.1	0.5	0.2
FCR CF[C]	54.9	30.6	0.8	7.9	0.6	2.1	1.2	0.1	0.5	0.2

[a]dl-below the detection limit.

The HF and HCl solution used in this study could remove almost all of the MM excluding inherent submicron minerals, organic sulfur, and carboxylate salts (organically associated inorganic elements)[10,17] accounting for 5 wt %. The general formula of carboxylate salts is as follows M(RCOO)n, where M is cations such as Mg^{2+}, Ca^{2+}, Na$^+$, and NH$_4^+$.

After pyrolysis at 500 °C, the IM and VM contents of the chars were reduced as a result of evaporation and devolatilization mechanisms, respectively. On the other hand, the AY % and fixed carbon contents are higher for all char samples, which is typical for SA feed-coals in the pyrolysis zone of the fixed-bed gasifier (T = 500 °C).[16,17] However, an anomaly is seen with regard to the FC of the chars of the FCR CF and ROSH blends, which indicates a possible enhancement of FC conversion by the ROSH composite.

Ultimate results (Table 1) indicate that the organic composition of macerals in the FCR and FCR D samples remains unchanged, which could suggest minimal FCR oxidation during demineralization, while the FCR CF sample comprised slightly less carbon and higher nitrogen and oxygen percentages. The variations could be correlated to possible slight oxidation, as well as nitrogen cross-linkage by ammonium acetate during the chemical fractionation experiments. As expected, the chars had a decrease in oxygen (O) and hydrogen (H) percentages, as well as an increase in carbon and nitrogen percentages, as a result of pyrolysis reactions. These results are consistent with those reported by Roets et al.[16] for coal demineralization and low-temperature pyrolytic chars for chemical fractionation of SA Highveld coals.[16]

The total sulfur (TS) content slightly increased with an increase in AY % of the density-separated fractions, while it remained constant for FCR D and decreased slightly for FCR CF indicating that the sulfur in the FCR residue produced during the chemical fractionation experiments is associated with extraneous pyrite and an organic carbon matrix (organic sulfur). With the addition of ROSH, TS remained constant which can be attributed to S capturing by Ca(OH)$_2$ to form anhydrite (CaSO$_4$), bassanite (CaSO$_4$·1/2H$_2$O), and gypsum (CaSO$_4$·2H$_2$O) [4].

The higher proportions of % AY values for the FCR, Fl 1.9, Sl 1.9, and FCR CF indicated by the proximate results could imply the presence of AAEM and metallic elements (Na, K, Ca, Mg, and Fe) associated with the cleat minerals (dolomite, calcite, and pyrite), EMs (dolomite, calcite, and pyrite), inherent minerals (dolomite, calcite, and pyrite), and non-mineral inorganics which could catalyze the pyrolysis reactions to yield higher carbon conversion during pyrolysis. Also, the higher proportions of H and O could imply higher carbon conversion during pyrolysis due to sufficient H for retarding free radicals and oxidation of char to form carbon gases.

3.2. XRF Analysis. XRF results for the ashes of the coal samples with and without ROSH composite, along with their corresponding chars, are presented in Table 2. The ashes of these samples comprised mainly SiO$_2$, Al$_2$O$_3$, CaO, SO$_3$, Fe$_2$O$_3$, and MgO with minor percentages of TiO$_2$, K$_2$O, Na$_2$O, and P$_2$O$_5$ which are consistent with the ash composition of SA feed-coals to commercial gasifiers.[26,27] Mphahlele et al.[28] found that higher concentrations of trace elements (Co, Zn, As, Rb, Sr, Zr, Ag, Cd, Ba, In, and Sn) and rare earth element (Y) are concentrated in the density-separated fractions of the FCR samples compared to the typical concentrations for SA Highveld ROM coals, as reported by Wagner and Hlatshwayo.[29] This could be associated with health and environmental issues during the storage of FCR samples in stockpiles and slime dams.

According to Hower et al.,[30] coal fines contain higher proportions of toxic trace elements (As, Cd, Cu, Hg, Mo, Pb, Sb, Zn, Cr, Ni, and Gd) which are associated with nanosulfide minerals. Also, these fines comprised higher proportions of rare earth elements which are linked to the nano monazite (Ce, La, Th, Nd, and Y) PO$_4$ and nano xenotime (Y and Er) PO$_4$.[30] Both significant contents of trace elements and rare earth elements present in the coal fine wastes have negative impacts on human health and the environment and should be recovered from coal ash using hydrometallurgical methods prior to either storage, disposal, or utilization in thermal processes under suitable operating conditions.

A decrease in major inorganic elements percentages in the ash of FCR D (except for Fe$_2$O$_3$, TiO$_2$, and Na$_2$O) is associated with the dissolution of MM by HCl and HF, while the decrease in CaO and MgO in the FCR CF indicates that dolomite and calcite associated with these inorganic elements exist predominantly in coals in acid soluble form, as ion-exchangeable cation, chelates, and cleat minerals.[17]
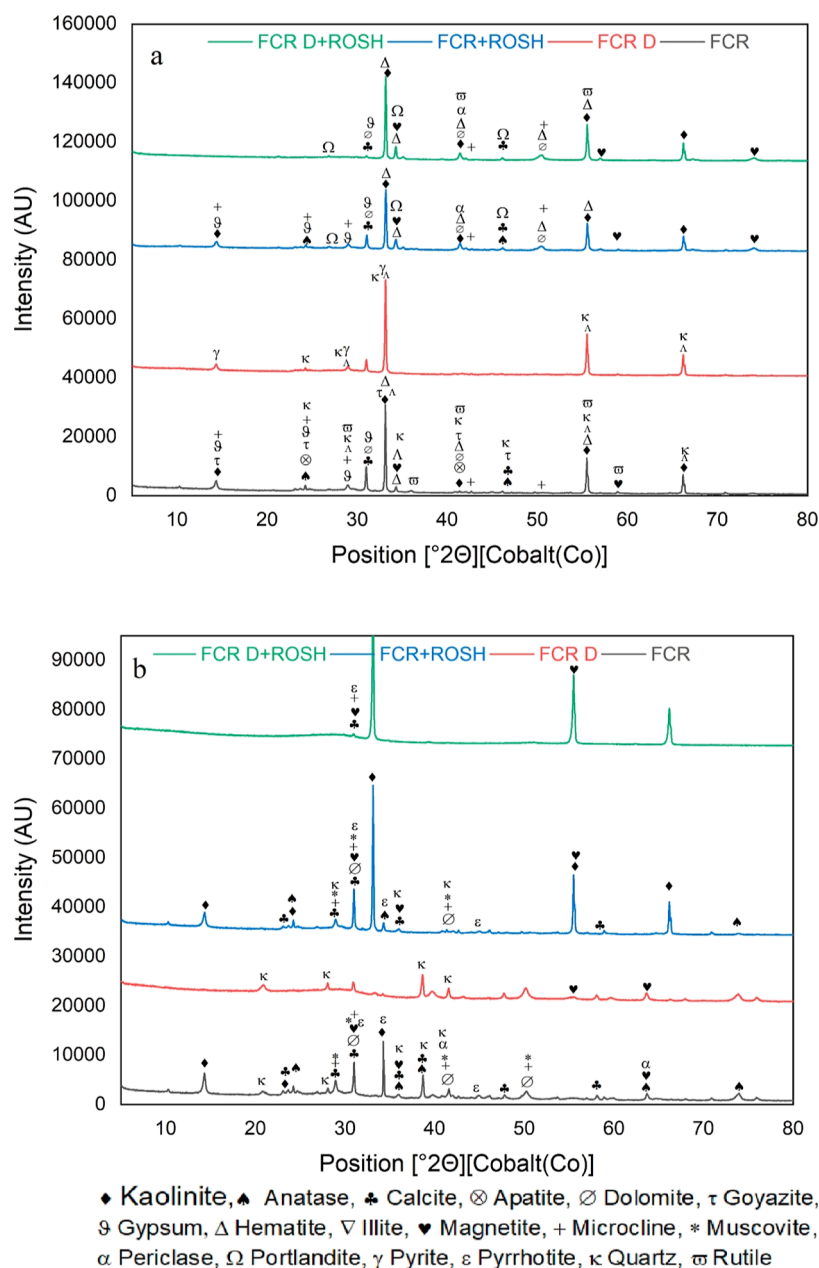
Figure 2. Diffractograms of (a) FCR and demineralized FCR along with their ROSH blends and (b) chars of FCR and demineralized FCR along with their ROSH blends.

As expected, variations in the compositions of the ashes of coal and ROSH composite blend samples illustrate higher proportions of CaO, Fe_2O_3, and MgO due to the addition of $Ca(OH)_2$, Fe_2O_3, and MgO to the FCR samples. In all instances, higher percentages of sulfur as SO_3 have been reported for samples with ROSH and FCR blends. This emphasizes the occurrence of sulfur encapsulation mechanisms by calcium oxide (CaO) from dehydroxylation of $Ca(OH)_2$ and the interaction of organic sulfur, pyrite, and organic Ca to form $CaSO_4$.[4] Furthermore, the occurrence of the sulfur encapsulation by added $Ca(OH)_2$ to the FCR samples could interfere with pyrolysis reactions and subsequently reduce the formation of pyrolytic products.

The presence of higher proportions of Ca, Mg, and Fe elements in the ashes of all the FCR samples without the FCR blends and the FCR CF sample implies that these inorganic elements could potentially catalyze the pyrolysis reactions which are linked to the dolomite, calcite, and pyrite cleats present in these samples.

3.3. XRD Analysis. The proportions of major and minor minerals of the FCR, treated FCR coal samples, FCR + ROSH and FCR D + ROSH, along with their corresponding chars are presented in Figure 2 and Table 3. In general, all samples without ROSH addition are primarily amorphous except for the Sl 1.9 and FCR CF samples, which showed a 40 wt % amorphous content indicating their richness in crystalline minerals. The XRD analysis for the FCR D indicates a 98% amorphous content due to the dissolution of all MM excluding inherent submicron pyrite, organic sulfur, and carboxylate salts.[17] XRD results indicate that the FCR, Fl 1.5, Fl 1.9, Sl 1.9, FCR CF, and FCR D contain 39.3, 13.4, 28.9, 59.7, 38.7, and 1.8% MM contents, respectively (Table 3). Also, the XRD

Table 3. Mineral Composition for FCR, Beneficiated Fractions, Acid-Washed Residues, and Their ROSH Blends along with Their Corresponding Chars[a]

mineral (wt %)	Kao	Ana	Ap	Cal	Dol	Goy	Gyp	Hem	Ill	Mag	Mic	Mus	Per	Por	Pyr	Pyrr	Qua	Rut	Amo	MM	total
FCR	21.5	0.1	0.1	3.0	4.3	0.1	0.3	0.4	1.0	0.0	0.1	1.1	0.1	-	0.6	-	7.7	0.1	60.7	39.3	100.0
FCR[C]	13.1	0.2	-	1.9	1.9	-	-	9.7	-	0.4	0.6	1.1	0.1	-	-	0.1	9.8	0.0	71.0	29.2	100.2
FCR + ROSH	22.4	0.2	0.0	2.7	3.8	0.0	0.6	-	0.5	0.2	0.4	-	7.7	3.0	0.0	-	8.2	-	40.6	59.4	100.0
FCR + ROSH[C]	11.5	0.2	-	5.8	0.8	-	-	-	-	3.8	0.3	1.2	5.0	-	-	0.3	7.1	0.0	64.1	36	100.1
Fl 1.5	8.3	0.0	0.0	0.4	0.3	0.0	0.2	0.0	0.9	0.1	0.2	0.9	-	-	0.2	-	2.8	-	86.6	13.4	100.0
Fl 1.5[C]	7.9	0.2	-	0.0	0.0	-	-	-	-	0.2	0.1	-	0.0	-	-	0.1	5.3	0.1	85.2	14.8	100.0
Fl 1.9	14.8	0.2	0	1.7	1.0	0.1	0.5	0.1	2.6	0.4	0.5	1.1	-	-	0.3	-	6.5	0.2	71.1	28.9	100.0
Fl 1.9[C]	8.5	0.3	-	0.0	0.2	0.2	-	-	-	0.3	0.6	-	0.2	-	-	0.0	7.0	0.0	81.8	18.2	100.0
Sl 1.9	27.3	0.2	0	4.8	1.7	0.2	1.1	0.2	5.5	0.9	1.0	1.2	-	-	0.9	-	15.6	0.3	40.3	59.7	100.0
Sl 1.9[C]	11.4	0.2	-	0.1	0.2	-	-	-	-	0.2	0.5	-	0	-	-	0.2	7.4	0.1	78.5	21.5	100.0
FCR D	-	-	-	-	-	-	-	-	-	-	-	-	-	-	1.8	-	-	-	98.2	1.8	100.0
FCR D[C]	0	0	0	0	0	0	0	0	-	0.1	0	0	0.2	-	-	0.2	0.5	0	99	1	100.0
FCR D + ROSH	1.3	0	0	1.1	-	0	0.2	10.4	0.7	0	0.8	-	9.4	5.1	-	-	2.4	0.1	68.5	31.5	100.0
FCR D + ROSH[C]	0	0	0	5.4	0	-	-	-	-	3.4	0.1	0	4.8	-	-	0.4	0.8	0	85.1	14.9	100.0
FCR CF	26.2	-	-	-	-	-	-	0.1	-	1.2	0.6	1.7	-	-	-	-	8.9	-	61.3	38.7	100.0
FCR CF[C]	7.4	0.1	-	0	-	-	-	-	-	0.2	0	0	0.1	-	-	0.1	4.1	0	88	12	100.0

[a]Kao-kaolinite, Ana-anatase, Ap-apatite, Cal-calcite, Dol-dolomite, Goy-goyazite, Gyp-gypsum, Hem-hematite, Ill-illite, Mag-magnetite, Mic-microcline, Mus-muscovite, Per-periclase, Por-portlandite, Pyr-pyrite, Pyrr-pyrrhotite, Qua-quartz, Rut-rutile, Amo-amorphous, "-"-not detected, and [C]-char.

detected traces of anatase (TiO_2), apatite [$Ca_5(PO_4)^{3+}$(F,Cl, or OH)], goyazite [$SrAl_3(PO_4)(PO_3OH)(OH)_6$], microcline ($KAlSi_3O_8$), rutile ($TiO_2$), and muscovite $(KF)_2(Al_2O_3)_3(SiO_2)_6(H_2O)$ in the case of FCR CF. These results are consistent with those of SA feed-coals and their density-separated fractions reported by Rautenbach et al.[12] Raman studies performed on FCR in the previous study by Mphahlele et al.[24] confirmed the presence of minerals detected by XRD in lower proportions.

Higher proportions of MM contents in Sl 1.9 and FCR are associated with higher total proportions of fluxing cleat minerals (calcite, dolomite, and pyrite) (>7%) compared to those of other beneficiated FCR samples. These higher cleat mineral contents are possibly responsible for the catalytic effect of pyrolysis reactions to produce higher carbon conversion values. On the other hand, the lowest or zero fluxing cleat mineral contents contained in the Fl 1.5, FCR CF, and FCR D imply that these beneficiated samples can achieve lower carbon conversion values during pyrolysis.

These samples are mainly made up of kaolinite ($Al_2Si_2O_5(OH)_4$) with lesser proportions of quartz (SiO_2) followed by dolomite and calcite and minor proportions of pyrite and illite $((K,H_3O)(Al,Mg,Fe)_2(Si,Al)_4O_{10}[(OH)_2, (H_2O)])$. The presence of traces of hematite (Fe_2O_3), magnetite (Fe_3O_4), anhydrite ($CaSO_4$), and gypsum ($CaSO_4 \cdot 2H_2O$) in the FCR sample and its density-separated fractions are derived from the spontaneous combustion of the FCR sample which resulted in oxidation of pyrite[26] and interaction of inherent pyrite, organic sulfur, and organic calcium[4] during the storage of these coal fines at the Highveld coal fine disposal site. These XRD results for the FCR sample and its density-separated fractions are consistent with those of SA Highveld coals.[11,16,17] In the case of FCR D and FCR CF, similar trends of minerals in the demineralized and chemically fractionated samples are reported in past studies by Raghoo.[17]

Calcite, dolomite, and pyrite in the FCR sample are linked to the cleats and could release Ca, Mg, and Fe to catalyze the pyrolysis reactions and achieve higher pyrolytic product efficiencies. According to Rautenbach et al.[12] the >1.9 g/cm^3 sink samples are characterized by the highest proportions of calcite, dolomite, siderite, and pyrite cleats and zero % or lowest proportion of inherent minerals compared to feed-coal and its density separated fractions. This could imply that Sl 1.9 evaluated in this study may achieve the highest carbon conversion value during pyrolysis.

XRD results for the prepared chars indicate different pathways for partial mineral transformation for both samples with and without the addition of ROSH composite addition. As expected, all char samples reported an increase in the percentage of amorphous materials, except for the char of the Fl 1.5 sample which contains 100% inherent MM.[12] The increase in amorphous material is associated with the partial transformation of kaolinite by losing water of hydration to form metakoalinite at 500 °C.[31,32] While this is the case for every sample, this transformation of kaolinite is minimal for the Fl 1.5 samples, which, combined with the loss of volatiles, is responsible for a decrease in the percentage of amorphous materials.

3.4. Chemical Fractionation Procedure. The % of leachable elements in FCR by deionized water, 1 M ammonium acetate ($NH_4CH_3CO_2$), and 1 M hydrochloric acid (HCl) solutions are presented in Table 4. Water leaching removed the Ca, Mg, Na, K, and S ions dissolved in pore

Table 4. Leachability of Inorganic Elements in FCR by Deionized Water, 1 M NH₄CH₃CO₂, and 1 M HCl Solutions

element	leach liquor composition			% leachable element		
	deionized water (mg/L)	1 M $NH_4CH_3CO_2$ (mg/L)	1 M HCl (mg/L)	deionized water (wt %)	1 M $NH_4CH_3CO_2$ (wt %)	1 M HCl (wt %)
Al	0.0	0.0	648.4	0.0	0.0	10.3
Ca	231.1	2726.1	2934.4	3.3	39.0	42.0
Fe	0.0	0.0	1119.9	0.0	0.0	91.0
K	7.6	15.1	13.4	1.9	3.7	3.3
Mg	39.0	139.1	605.2	3.1	10.9	47.4
Mn	0.0	6.9	30.3	0.0	14.8	65.1
Na	222.7	116.4	33.4	56.2	29.4	8.4
P	0.0	0.0	126.2	0.0	0.0	87.4
S	429.9	36.3	19.1	24.6	2.1	1.1
Si	4.9	4.5	181.3	0.0	0.0	0.7
Ti	0.0	0.0	1.0	0.0	0.0	0.1

waters within the FCR structure. The inorganic elements associated with salts of carboxylic acids removed by 1 M $NH_4CH_3CO_2$ solution were primarily Ca with a lesser removal percentage for Na followed by Mn, Mg, K, and S, while 1 M HCl solution leached primarily Fe, P, and Mn and lesser proportions of Mg, Ca, Al, Na. K, S, and Si. The latter elements are associated with minerals and mineraloids in FCR such as carbonates, hydroxides, oxides, organically associated inorganic elements as well as submicron clays contaminated with Ti and Mn.[4,17]

The largest proportion of Na ions (ca. 60%) in FCR exists as cations dissolved in pore waters, followed by Na associated with salts of carboxylic acids and submicrometer clay and carbonates. However, Fe (ca. 90%) is predominantly associated with submicrometer pyrite in the FCR sample. The absence of Fe in the water-leaching liquor illustrates minimal oxidation of pyrite during the storage of FCR in slurry dams. These findings are in agreement with Raghoo[17] on SA feed-coals to gasifiers. The carboxylic acid salts, submicron minerals, and ions dissolved in pore waters, especially Fe and Ca are linked with bond cleavage reactions during pyrolysis to form various aliphatic and aromatic structures.[33] As a result, their absence in the FCR CF sample could lower the carbon conversion.

3.5. BET Surface Area Analysis. CO_2 and N_2 surface area results of the FCR sample, the beneficiated fractions, and their corresponding chars and chars of FCR + ROSH and FCR D + ROSH are presented in Table 5. Samples with a high % AY

Table 5. BET Surface Area Results for FCR, Beneficiated Fractions, Acid-Washed Residues, and ROSH Blends along with Their Corresponding Chars

sample	CO_2 (m²/g)	N_2 (m²/g)
FCR	76.6	5.1
FCR[C]	91.4	10.1
FCR + ROSH[C]	72.7	12.0
Fl 1.5	73.4	3.6
Fl 1.5[C]	93.3	3.3
Fl 1.9	63.3	4.5
Fl 1.9[C]	85.6	3.9
Sl 1.9	54.2	4.9
Sl 1.9[C]	80.9	5.8
FCR D[C]	141.2	2.7
FCR D + ROSH[C]	112.3	13.6
FCR CF[C]	119.4	3.4

reported the lowest mesopore structures due to the higher proportions of low porosity minerals.[34] An increase in the CO_2 and N_2 surface areas of all samples illustrates the development of pores and change in the pore structures during pyrolysis due to the evolution of volatile compounds. However, the yielded ROSH chars with a reduced surface area could be due to the dilution by Fe_2O_3 which comprises a low-surface area. Shivakumara et al.[35] found the surface area of α-Fe_2O_3 to be less than 1 m²/g. The largest CO_2 surface area for FCR D followed by FCR CF could be attributed to the absence of minerals, such as quartz. However, the N_2 surface area for the acid-washed samples was the lowest, which indicates collapsing of mesopores during pyrolysis. It can be seen that the AY affects the structural properties of the coal and its chars. The fine nature of the added commercial [MgO, Fe_2O_3, and $Ca(OH)_2$] can contribute significantly to the surface area and mesopore structures and hence the increased mesopore surface area for ROSH char samples.

3.6. Pyrolytic Product Yields. *3.6.1. Char Yield.* The char yields for FCR, FCR CF, and FCR D samples in Figure 3 presented on a dry ash-free basis indicate the lowest carbon conversion (i.e., high char yield) for the FCR CF sample due to the partial dissolution of calcite, dolomite, and pyrite cleats, nonmineral inorganics, and extraneous and inherent fluxing minerals as well as carbonates and sulfate formation as the
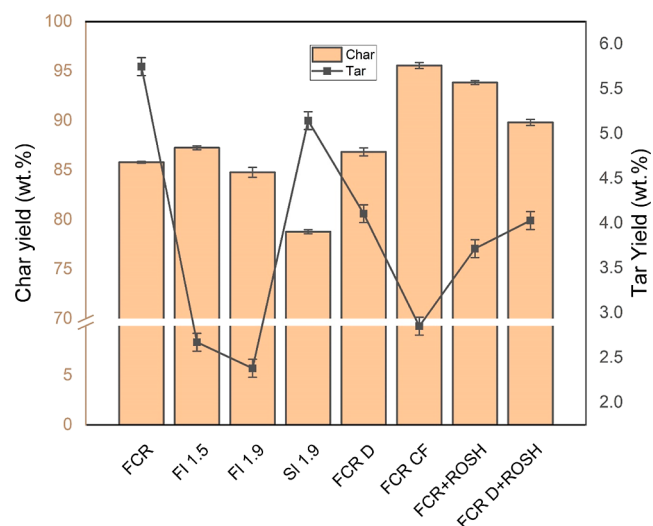
Figure 3. Product distribution during pyrolysis of FCR and its beneficiated fractions and FCR/FCR D and ROSH blends at 500 °C.

Table 6. List of Possible Reactions Taking Place during Pyrolysis of FCR, Beneficiated Fractions, Acid-Washed Residues, and ROSH Blends

	MgO	Ca(OH)$_2$
activation reaction	$6MgO_{(s)} + 2N_{2(g)} \rightarrow 3O_2 + 2Mg_3N_{2(s)}$ $\Delta H = -462.81 \text{ kJ/mol}, T = 773 \text{ K}$ (6)	$Ca(OH)_{2(s)} \rightarrow CaO_{(s)} + H_2O_{(g)}$ $\Delta H = 788.2 \text{ kJ/mol}, T = 673 \text{ K}$ (8)
reactions	$MgO_{(s)} + H_2S_{(g)} \rightarrow MgS_{(s)} + H_2O_{(g)}$ (7)	$CaO_{(s)} + CO_{2(g)} \rightarrow CaCO_{3(s)}$ (9) $CaO_{(s)} + SO_{3(g)} \rightarrow CaSO_{4(s)}$ (10)
	Fe$_2$O$_3$	**Fe$_2$O$_3$ alternative**
reduction/activation reaction	$3Fe_2O_3 + H_2 \rightarrow 2Fe_3O_4 + H_2O$ $\Delta H = 533.9 \text{ kJ/mol}, T = 533 \text{ K}$ (11)	
reactions	$3Fe_3O_4 + H_2S \rightarrow SO_{2(g)} + 9FeO + H_2O$ (12) $FeO_{(s)} + H_2S_{(g)} \rightarrow FeS_{(s)} + H_2O_{(g)}$ (13) $Fe_{(s)} + H_2S_{(g)} \rightarrow FeS_{(s)} + H_{2(g)}$ (14)	$Fe_2O_3 + CO/C \rightarrow Fe_{(s)} + FeO_{(s)} + CO_{2(g)}$ (15) $Fe_{(s)} + Char_{(s)} + CO_{2(g)} \rightarrow Fe-O-C_{(s)} + CO_{(g)}$ (16) $Fe-O-C_{(s)} \rightarrow FeC_{(s)} + CO_{(g)}$ (17)

artifacts. The ICP analysis of the leachates confirms the dissolution of sulfur, calcium, iron, magnesium, and potassium species by the CF procedure. These have been associated with enhancements of several carbon conversion reaction mechanisms such as depolymerization and dehydroxylation reactions, particularly those of intimate or organic association with the carbon matrix.[36] The presence of higher proportions of calcite, dolomite, and pyrite cleats as well as Ca/Mg carboxylates in the FCR sample catalyzed pyrolysis reactions and may result in higher carbon conversion. Interestingly, pyrolysis of the FCR D sample yielded a lower char yield than FCR CF even with the almost complete removal of all MM. The slightly higher carbon conversion for FCR D could be associated with the high-surface area and recalcitrant inherent pyrite. The latter contributes to the conversion of carbon via the catalytic Boudouard reaction (eqs 15−17). However, the former allows for the transport of intermediate vapors through the developed pores with minimal secondary polymerization reactions.[37] This illustrates that extraneous clays and quartz predominantly present in FCR CF contribute minimally to carbon conversion at 500 °C. Nonetheless, the demineralization of FCR did not significantly increase the carbon conversion (i.e., Y_{char} FCR ≈ Y_{char} FCR D). Similar findings were obtained by Roets et al.[16] during the pyrolysis of acid-washed SA coals. This can be attributed to the removal of calcite, dolomite, pyrite cleats, and nonmineral inorganics which can catalyze the pyrolysis reactions during the demineralization experiments of the FCR sample.

Although density separation of the FCR sample produced fractions comprising different modes of occurrence of MM, the results should be used with caution since the liberation of macerals (coal organic matrix) also took place. Maceral groups have different pyrolytic characteristic temperatures, which also overlap and could mask the effects of MM. Nonetheless, some inferences can be made on the effect of the mode of occurrences of MM on the distribution of pyrolysis products. The lowest char yield (i.e., highest carbon conversion) was obtained for the Sl 1.9 sample followed by the FCR, Fl 1.5, and Fl 1.9 samples. Except for the Fl 1.9 sample, there is a better proportional relationship between the AY and the carbon conversion of these samples.

The higher proportions of gypsum (product of the interaction of organic Ca, organic S, and S) released from pyrite at 400 °C,[17] dolomite, calcite, apatite, and pyrite which

transform into reactive/catalytic Ca, Mg, and Fe species at 500 °C, can be attributed to the higher carbon conversion during pyrolysis.[4,34] The XRD results of the FCR and Sl 1.9 samples confirmed the presence of these reactive/catalytic Mg, Ca, and Fe minerals in the FCR and Sl 1.9 chars. Two possibilities exist for lower char yield for Fl 1.5 compared to Fl 1.9; (1) the presence of low proportions of cleat minerals associated intimately with the carbon matrix in the Fl 1.5 sample, and (2) the prominence of vitrinite macerals in the Fl 1.5 which have been associated with lower characteristic temperatures.[38]

Adding the ROSH composite to the FCR and FCR D samples led to an increase in char yield %. A comparison between the char yields of FCR + ROSH and FCR D indicates that increasing the overall Ca and Fe contents reduced carbon conversion during pyrolysis. This can be attributed to capturing of CO_2 by either $Ca(OH)_2$ added to FCR and FCR D to form $CaCO_3$ in the blend chars during pyrolysis (eqs 8 and 9 in Table 6, and Table 3).[39] Also reactive Fe from the reduction of Fe_2O_3 in the blend chars can react with CO_2 to form Fe−O−C and FeC in the char samples (eqs 15−17).[39] The formed Fe−O−C and FeC formed in the blend chars were not detected by XRD due to their crystal size (<2 nm) as well as the equipment detection limit of <1% volume.[4] While Mg may form amorphous MgS or react with N_2 to form Mg_3N_2 (eqs 6 and 7).[39]

The presence of magnetite in the chars of FCR + ROSH and FCR D + ROSH can be associated with the reduction of the Fe_2O_3 in these ROSH blend samples, which resulted in catalyzing the pyrolysis reactions. The XRD results of the chars of FCR + ROSH and FCR D + ROSH showed the presence of calcite in these samples, which could derive from carbonation of intermediate CaO derived from dehydration of $Ca(OH)_2$.

3.7. Tar Yields. Pyrolytic tar yields indicate the highest tar yield for the FCR sample, followed by the FCR and FCR CF samples (Figure 3). Roets et al.[16] linked the lower tar yields by acid-treated samples to limited hydrogen transfer, usually facilitated by MM. In the case of inadequate H+ transfer, solidification or secondary polymerization reactions take place, which leads to the formation of char over tar. Although FCR D has lost 98% of its minerals including the cleat minerals, it still has a higher tar yield than FCR CF due to the higher BET surface area associated with the mineral matter removal. This is because acid washing created active oxygen sites and scattering of coal microstructure, making it unstable and susceptible to

thermal scission.[40] The lower tar yield for FCR CF is linked to the lower carbon conversion. The tar yields of the density-separated fractions were obtained in the order of FCR > Sl 1.9 > Fl 1.5 ≈ Fl 1.9. The tar was 10, 53, and 58 wt % lower than that of FCR for Sl 1.9, Fl 1.5, and Fl 1.9, respectively. This agrees with the correlation of EMs with carbon conversion. While inherent MM contributes to bond scission of polymerized structures, the hot ash layer by EMs promotes secondary cracking of intermediate vapors to form low-molecular-weight tars, thus more tars. Rautenbach et al.[12] found that float fractions (comparable to Fl 1.5) of SA feed-coals are free of mineral cleats while the sink fraction (comparable to Sl 1.9) is rich in rock fragments, calcite/dolomite/siderite/pyrite cleats, and carbominerites. Cleat minerals and carbominerites comprising pyrite, dolomite, and calcite released metallic Ca, Mg, and Fe to catalyze the pyrolysis reactions, which explains the increased tar yields for the FCR and Sl 1.9 samples.

Furthermore, the proportion of cleat fluxing minerals is higher for Sl 1.9 compared with Fl 1.9 and Fl 1.5 samples (Table 3). MgO and CaO [derived from dehydroxylation of $Ca(OH)_2$] promoted deoxygenation and cleavage of oxygen-containing bonds while Fe, derived from the reduction of Fe_2O_3 to Fe (eq 15), promotes deoxygenation of carboxylic functional groups via catalytic Boudouard reactions.[14] The addition of the ROSH composite to FCR D and FCR did not have a significant effect on the tar yields indicating that EMs do not contribute to the evolution of tars, but secondary reactions during transport of tar precursors through the hot ash layer.[41]

3.8. Tar Composition. The tar samples from the FCR, FCR + ROSH, and its beneficiated fractions obtained from pyrolysis tests at 500 °C were subjected to GC/MS measurements to identify the compounds present in the tars. A minimum of 100 organic compounds were detected with a 90% confidence level and were classified into six (6) chemical families (Figure 4), namely, 1-ring aromatic hydrocarbons (1-ringArH), aromatic and polycyclic aromatic hydrocarbons (PAHs), aliphatic hydrocarbons (aliphatic H), ethers and esters, alkylated fractions (i.e., alkyl-benzenes, alkyl-phenols, alkyl-indenes, and alkyl-naphthalenes), and nitrogen and inorganic element containing compounds [(N, inorganic)-

containing]. The relative peak area percentages (RA %) of these chemical families are used as a semiquantitative tool to compare the compositions of the obtained pyrolytic tars. In the case of the FCR, FCR D, and FCR CF samples, the RA % for PAHs was obtained in the order of FCR CF ≈ FCR D > FCR. However, the RA % for aliphatic hydrocarbons illustrated an FCR > FCR CF > FCR D trend opposite to the PAHs. This indicates that secondary reactions by MM present in the increasing order of FCR D > FCR CF > FCR contributed to the secondary cracking of the complex PAH structures into light gases and aliphatic hydrocarbons via side-chain decomposition and hydrocracking reactions. Ca, Mg, and Fe which are associated with the cleat minerals and nonmineral inorganics have been associated with the promotion of such reactions during pyrolysis.[14]

The higher proportions of ethers and esters for the FCR CF and FCR D samples suggest that deoxygenation and dehydroxylation reactions of tars are promoted by EMs through cleavage of C−O and C−H bonds by secondary volatiles−MM interaction.[42] The proportions of all alkylated fractions are almost the same between the FCR D and FCR CF samples, while lowest for the FCR indicating the contribution of water-soluble cations and salts of carboxylic acids toward thermal desorption and decomposition of alkylated compounds and prevention of cross-linking reactions.[43] The proportions of (N-inorganic)-containing compounds include sulfonated compounds, which could be attributed to the higher proportions of this group for FCR CF and FCR D due to the lower % AY comprising S-capturing capable minerals.

The evolution of 1-ring aromatic compounds relates to the cleavage of ether and methylene bridges associated with the aromatic nuclei occurring at lower temperatures.[44] These are the highest in the FCR D sample and not detectable in the FCR CF sample, which could be attributed to possible significant changes in the organic structure of FCR D.

In the case of density-separated fractions, the effect of MM interactions on tar composition is clear between Fl 1.5 and Sl 1.9. This is owed to the better liberation of MM between the two density-separated fractions. The proportion of PAHs and oxygenated (ethers and esters) compounds were higher in Fl 1.5, while both were lowest in the tar of Sl 1.9.

Besides the suggested deoxygenation reactions by inherent minerals, Sl 1.9 is rich in extraneous kaolinite. Like zeolites, the acid sites associated with extraneous kaolinite or metakaolinite in coal or char promoted the decomposition of PAHs and oxygenated compounds and enhanced the formation of alkylated fractions. The Sl 1.9 fraction is concentrated in oxygen-carrying minerals. These oxygen carriers inhibited the deoxygenation of intermediate volatiles by reacting directly with carbon via MM-char reaction pathways (eqs 16 and 17). For instance, Fe reacts with active oxygen sites which actives carbon sites and improves carbon conversion.[14] This reaction mechanism is also suggested by an increase in the number of oxygen-containing aromatic compounds in the FCR + ROSH blend.

The ROSH addition decreased the proportions of aliphatic hydrocarbons in the tars of FCR sample only but increased the proportions of PAHs, ether, and esters. This behavior suggests the promotion of recombination reactions by ROSH.[45] Since PAHs evolve from the thermal cracking of coal macro-molecular structure and thermal desorption of PAHs,[46] the higher proportions of PAHs in Fl 1.5, Fl 1.9, Sl 1.9, FCR CF, and FCR D are associated with the chemical compositions of
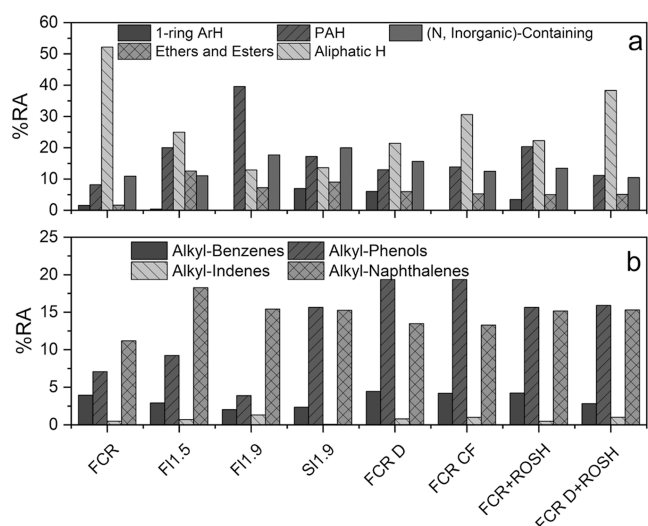
Figure 4. Distribution of chemical compounds during the pyrolysis of FCR and its beneficiated fractions and ROSH blends at 500 °C.

these samples. However, upon the addition of ROSH to FCR D, the PAHs proportions reduced slightly due to secondary catalytic cracking reactions of long-chain hydrocarbons and side chains associated with aromatic nuclei to form aliphatic hydrocarbons as well as dealkylated compounds.[44] Moreover, the addition of ROSH increased the proportions of alkylated compounds for both samples, illustrating the selectivity of these compounds over aliphatic hydrocarbons.

3.9. Simulated Distillation. The analysis for simulated distillation of tars obtained from pyrolysis of FCR, its beneficiated fractions, and blends of FCR and FCR D with ROSH at 500 °C are presented in Figure 5. The boiling point
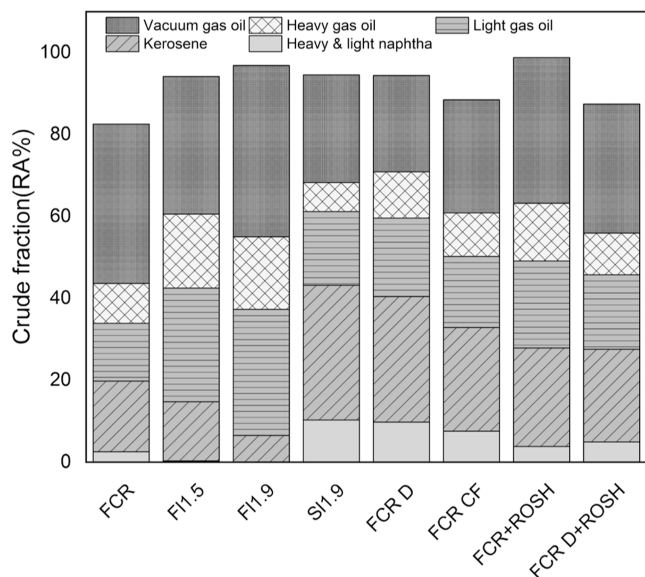
Figure 5. Crude fraction distribution of tars obtained during pyrolysis of FCR and its beneficiated fractions and ROSH blends at 500 °C.

differences were used to group proportions of light and heavy naphtha (90−180 °C), kerosene (180−230 °C), light gas oil (230−320 °C), heavy gas oil (320−375 °C), and vacuum gas oil across samples. The results indicate an increase in naphtha, kerosene, light gas, and heavy gas oil fractions in all samples except Fl 1.9. However, the vacuum gas oil decreased for the FCR D and FCR CF tars attributed to the absence of inherent MM responsible for depolymerization reactions.

The Fl 1.5 and Fl 1.9 samples comprising inherent MM and zero % of mineral cleats yielded the lowest fraction of naphtha,

kerosene, and light gas compared to Sl 1.9. The latter enhanced the secondary catalytic cracking reactions. The addition of ROSH to FCR sample did not increase the fraction of lower boiling point tar components, illustrating the inferiority of the secondary cracking reaction. This behavior could be attributed to the aromatization of tar precursors promoted by higher proportions of CaO from $Ca(OH)_2$ along with $CaCO_3$ formation.[34] The formation of $CaCO_3$ resulted in an increased char yield for these samples. Increasing the overall proportions of ROSH decreased the carbon conversion and increased the proportions of heavy tar fractions. This phenomenon was also seen for the FCR + ROSH sample where the fraction of lower boiling point tar components was reduced. The reduced fractions of light tars in Fl 1.5 (zero cleats) indicate that cleat minerals could have a higher potency for catalytic cracking of heavy compounds into lighter ones.

3.10. Activation Energy. The distribution of E_a with conversion and the average E_a for FCR and FCR D along with their corresponding blends with the ROSH composite are presented in Table 7. Although the average E_a is useful for understanding the general E_a requirement for the entire coal pyrolysis process, using it solely generalizes pyrolysis stages while concealing their reaction mechanisms. As a result, the emphasis is placed on x versus E_a trends.

In general, pyrolysis of FCR has a higher E_a in comparison to coal from other regions due to the different coal properties such as macerals and MM contents and their mode of occurrence.[47] The magnitudes of E_a varied with x which indicated the occurrence of multiple complex reactions involved in coal pyrolysis. Using the FCR sample as a benchmark, it is seen that E_a values increase with an increase in x and T which is ascribed to the cleavage of weaker bonds at lower temperatures due to their lower E_a requirement.

At $0.1 < x < 0.2$, FCR indicated the lowest E_a requirement for carbon conversion. The residual inherent pyrite (i.e., fluxing cleat mineral) in FCR D could be associated with the lower E_a for FCR D compared to FCR CF at this conversion range. The lower coefficient of determination (R^2) values are indicative of these reactions which is the case in previous studies that the occurrence of parallel reactions lower model linearity.[25] With the ROSH composite, E_a reduced for FCR while FCR D showed an increase of E_a at $x = 0.1$. However, at $x = 0.2$ the E_a for FCR D and FCR was equal, while that of FCR CF dropped.

At $0.3 < x < 0.7$ FCR indicated the highest E_a requirement which could be ascribed to the partial transformation of

Table 7. Activation Energy Distribution for FCR and Its Beneficial Fractions and ROSH Blends[a]

T (K)	X	FCR		FCR CF		FCR D		FCR + ROSH		FCR D + ROSH	
		E_a	R^2	E_a	R^2	E_a	R^2	E_a	R^2	E_a	R^2
405.55	0.1	251.4	1	291.5	0.9982	276.8	0.9993	233.4	0.9984	283.8	0.999
438.25	0.2	262.7	0.9979	267.9	0.9984	254.5	0.9997	277.1	0.9997	278.6	1
463.25	0.3	279.6	0.9928	268.9	0.9997	261.8	0.9995	295.5	0.9991	319.0	0.9991
490.95	0.4	293.9	0.9770	274.6	0.9995	279.0	0.9998	316.7	0.9943	421.5	0.9890
526.25	0.5	315.3	0.9650	295.4	0.9996	301.6	0.9979	355.5	0.9771	485.1	0.9626
568.55	0.6	349.6	0.9534	332.4	0.9997	324.7	0.9970	359.2	0.9601	475.1	0.9384
610.75	0.7	413.2	0.9798	391.1	0.9988	363.4	0.9966	362.9	0.9620	361.7	0.9710
670.75	0.8	409.3	0.9956	478.1	0.9985	403.4	0.9958	378.1	0.9749	881.7	0.9944
746.85	0.9	413.0	0.9910	537.1	0.9984	445.4	0.9948	1709.8	0.8219	1394.0	0.9786
average E_a (kJ/mol)		**332.0**		**348.5**		**323.4**		**476.5**		**544.5**	

[a]E_a—activation energy and R^2—coefficient of determination.

extraneous kaolinite, pyrite, dolomite, and calcite at $T > 500$ °C. The contribution of these EMs to the E_a is supported by the lowest E_a values for the FCR D sample until $x = 0.8$, $T = 670$ °C due to the low concentration of EMs whose transformation is highly endothermic as indicated in eqs 8 and 11. This behavior is more pronounced with the addition of ROSH composite, where a spike in E_a is observed for the FCR + ROSH and FCR D + ROSH at $x = 0.7$, $T = 610$ °C. This is linked to a new peak found by Shi et al.[48] at $T < 600$ °C attributing to calcium during analytical pyrolysis of Inner Mongolia coal/CaO mixtures which increased E_a in that zone. At $T > 700$ °C, highly endothermic reactions such as those in eqs 15 and 16 take place, which could be associated with the overall spike in E_a. These reaction mechanisms and E_a suggest that the decomposition of minerals composite and carbon matrix occurs almost parallel with minimal contribution to primary pyrolysis reactions. The change in yields and composition of pyrolytic products is ascribed to secondary pyrolysis reactions (i.e., depolymerization, polymerization, tar cracking, and dehydroxylation) as the intermediate vapor evolves and contacts the hot ash particle of EMs.

4. CONCLUSIONS

A study to evaluate the effect of reactive oxides and hydroxide composite of fluxing EMs and the mode of occurrence of MM on the pyrolysis behavior of FCR was evaluated by the yields of tar and char along with apparent activation energy.

Demineralization, chemical fractionation, and density separation procedures produced samples with various types of modes of occurrences of MM, which provided insights into their effects on pyrolysis reactions.

The highest carbon conversion (char yield = 78.9 wt % and tar yield = 5.1 wt %) was achieved for FCR and decreased in the order FCR (char yield = 78.9 wt % and tar yield = 5.1 wt %) > FCR D (char yield = 86.8 wt % and tar yield = 4.1 wt %) and FCR CF (char yield = 95.6 wt % and tar yield = 2.9 wt %) due to the prominence of extraneous, nonmineral inorganics, and inherent dolomite/calcite/pyrite cleats. Although the ROSH composites do not contribute significantly to carbon conversion, they facilitate secondary cracking reactions during the FCR pyrolysis. Artifacts of EMs (metakaolinite, calcite, and dolomite) [carbonation with $Ca(OH)_2$ and (MgO)] with hindering effects were formed in the blend chars during low-temperature pyrolysis and navigated the reaction pathways. On the other hand, magnetite $(FeO \cdot Fe_2O_3)$ with a catalytic effect was formed in the blend chars due to the Fe_2O_3 reduction. The highest tar yield of 5.7 wt % was achieved for FCR followed by 5.1 wt % for Sl 1.9, 4.1 wt % for FCR D while Fl 1.9 achieved the lowest tar yield of 2.4 wt % due to the prominence of nonmineral inorganics and inherent dolomite/calcite/pyrite mineral cleats in FCR and Sl 1.9 with a catalytic cracking characteristics.

The highest inherent MM [nonmineral inorganics, organic Ca/Mg/Fe (carboxylate salts), and dolomite/calcite/pyrite cleats] contents in Sl 1.9 facilitated the conversion of carbon matrix to volatile compounds during pyrolysis as shown by higher carbon conversion for Sl 1.9 compared with FCR. However, secondary reactions were facilitated by the presence and amount of extraneous ROSH and nonmineral inorganics present in FCR. These MMs enhance dealkylation and hydrocracking reactions to produce aromatic and aliphatic hydrocarbons.

Excess oxygen-carrying minerals inhibit deoxygenation reactions during low-temperature pyrolysis. The addition of ROSH composite to the FCR sample and FCR D increases the proportions of oxygen carriers, which inhibits dehydroxylation and deoxygenation reactions but enhances secondary dealkylation and cracking to form aromatic and aliphatic compounds. The addition of ROSH composites to the FCR samples increased the average E_a values from 332.0 to 476.5 kJ/mol for FCR and from 323.4 to 544.4 kJ/mol for FCR D due to the initial dehydration of $Ca(OH)_2$ and reduction of Fe_2O_3.

This work provides insights into the distribution and mode of occurrence of MM and their effects on pyrolysis reaction mechanisms along with the effects of cleavage minerals and carboxylate salts during utilization of FCR in the global thermochemical processes. This can reduce health and environmental issues, as well as higher FCR disposal costs. Since MM and the carbon matrix may interact differently at high temperatures and in different proportions, investigations into the effects of temperature and proportions of EMs as indigenous minerals or in their oxides and hydrated oxide forms may be an insightful future study. Furthermore, the high-resolution transmission electron microscopy and QEMSCAN analyses should be used to qualify and quantify nanominerals (microcleats) with catalytic and hindering effects in the pyrolytic chars. Also the effect of mineral distribution across the coal particle size on the pyrolytic product yields should be investigated during pyrolysis.

■ AUTHOR INFORMATION

Corresponding Author

Katlego Mphahlele − *Centre of Excellence in Carbon-Based Fuels, School of Chemical and Mineral Engineering, North-West University, Potchefstroom 2520, South Africa;* ⊙ orcid.org/0000-0003-2677-3928; Phone: +27 81 055 9653; Email: katl.mph@gmail.com

Authors

Ratale Henry Matjie − *Centre of Excellence in Carbon-Based Fuels, School of Chemical and Mineral Engineering, North-West University, Potchefstroom 2520, South Africa;* ⊙ orcid.org/0000-0002-2839-3729

John Reginald Bunt − *Centre of Excellence in Carbon-Based Fuels, School of Chemical and Mineral Engineering, North-West University, Potchefstroom 2520, South Africa;* ⊙ orcid.org/0000-0003-3051-2528

Complete contact information is available at:
https://pubs.acs.org/10.1021/acsomega.3c05462

Notes

The authors declare no competing financial interest.

from Set point laboratories are thanked for assistance with different aspects of the analytical techniques.

■ REFERENCES

(1) Statistics South Africa. *Mineral Accounts 1980−2008 Final 7 March.Doc|Enhanced Reader*, 2011;.

(2) Leokaoke, N. T.; Bunt, J. R.; Neomagus, H. W. J. P.; Waanders, F. B.; Strydom, C. A. CO$_2$ Reactivity of Briquettes Derived from Discard Inertinite-rich Highveld Coal Using Lignosulphonate and Resin as Binders. *J. South. Afr. Inst. Min. Metall.* **2019**, *119*, 847−854.

(3) Isaac, K.; Bada, S. O. The Co-combustion Performance and Reaction Kinetics of Refuse Derived Fuels with South African high Ash Coal. *Heliyon* **2020**, *6*, No. e03309.

(4) Rautenbach, R.; Strydom, C. A.; Bunt, J. R.; Matjie, R. H.; Campbell, Q. P.; Van Alphen, C. Mineralogical, Chemical, and Petrographic Properties of Selected South African Power Stations Feed Coals and Their Corresponding Density Separated Fractions Using Float-Sink and Reflux Classification Methods. *Int. J. Coal Prep. Util.* **2019**, *39*, 421−446.

(5) Singh, U.; Sharma, N.; Mahapatra, S. S. Environmental Life Cycle Assessment of Indian Coal-Fired Power Plants. *Int. J. Coal Sci. Technol.* **2016**, 3 (2), 215−225.

(6) Shekarian, Y.; Rahimi, E.; Shekarian, N.; Rezaee, M.; Roghanchi, P. An Analysis of Contributing Mining Factors in Coal Workers' Pneumoconiosis Prevalence in the United States Coal Mines. *Int. J. Coal Sci. Technol.* **2021**, 8 (6), 1227−1237.

(7) Nádudvari, A.; Cabała, J.; Marynowski, L.; Jabłońska, M.; Dziurowicz, M.; Malczewski, D.; Kozielska, B.; Siupka, P.; Piotrowska-Seget, Z.; Simoneit, B. R.; Szczyrba, M. High Concentrations of HgS, MeHg and Toxic Gas Emissions in Thermally Affected Waste Dumps from Hard Coal Mining in Poland. *J. Hazard. Mater.* **2022**, *431*, 128542.

(8) Frandsen, F.; Dam-Johansen, K.; Rasmussen, P. Trace Elements from Combustion and Gasification of Coal—an Equilibrium Approach. *Prog. Energy Combust. Sci.* **1994**, *20* (2), 115−138.

(9) Pone, J. D. N.; Hein, K. A. A.; Stracher, G. B.; Annegarn, H. J.; Finkleman, R. B.; Blake, D. R.; McCormack, J. K.; Schroeder, P. The Spontaneous Combustion of Coal and Its By-products in the Witbank and Sasolburg Coalfields of South Africa. *Int. J. Coal Geol.* **2007**, *72*, 124−140.

(10) Ward, C. R. Analysis, Origin and Significance of Mineral-Matter in Coal: An Updated Review. *Int. J. Coal Geol.* **2016**, *165*, 1−27.

(11) Matjie, R. H.; French, D.; Ward, C. R.; Pistorius, P. C.; Li, Z. Behaviour of Coal Mineral-Matter In Sintering and Slagging of Ash During the Gasification Process. *Fuel Process. Technol.* **2011**, *92*, 1426−1433.

(12) Rautenbach, R.; Matjie, R. H.; Strydom, C. A.; Bunt, J. R.; Ward, C. R.; French, D.; Van Alphen, C. Evaluation of Mineral-Matter Transformations in Low-Temperature Ashes of South African Coal Feedstock Samples and Their Density Separated Cuts Using High-Temperature X-ray Diffraction. *Int. J. Coal Prep. Util.* **2020**, *40*, 320−347.

(13) Fu, Y.; Guo, Y.; Zhang, K. Effect of Three Different Catalysts (KCl, CaO, and Fe$_2$O$_3$) on the Reactivity and Mechanism of Low-Rank Coal Pyrolysis. *Energy Fuels* **2016**, *30*, 2428−2433.

(14) He, R.; Deng, J.; Deng, X.; Xie, X.; Li, Y.; Yuan, S. Effects of Alkali and Alkaline Earth Metals of Inherent Minerals on Fe-Catalyzed Coal Pyrolysis. *Energy* **2022**, *238*, 121985.

(15) Sun, B.; Huang, X.; Huang, H.; Zhang, X.; Shang, W.; Sun, S.; Dai, Z.; Li, K. Preparation of Iron-Based Catalysts by Mechanical Solid-Phase Ball Milling and Their Applications in Cohydrogenation of Coal and Petrochemical Coking Residual Oil. *ACS Omega* **2023**, *8*, 25134−25141.

(16) Roets, L.; Strydom, C. A.; Bunt, J. R.; Neomagus, H. W. J. P.; van Niekerk, D. The effect of acid washing on the pyrolysis products derived from a vitrinite-rich bituminous coal. *J. Anal. Appl. Pyrolysis* **2015**, *116*, 142−151.

(17) Raghoo, M. Volatilization of Aluminium and Silicon Species from a Highveld Coal. Ph.D. Thesis, North West University, South Africa, 2010.

(18) Roets, L.; Bunt, J. R.; Neomagus, H. W. J. P.; Van Niekerk, D. An Evaluation of a New Automated Duplicate-Sample Fischer Assay Setup According to ISO/ASTM Standards and Analysis of The Tar Fraction. *J. Anal. Appl. Pyrolysis* **2014**, *106*, 190−196.

(19) Liu, Q.; Hu, H.; Zhou, Q.; Zhu, S.; Chen, G. Effect of Inorganic Matter on Reactivity and Kinetics of Coal Pyrolysis. *Fuel* **2004**, *83*, 713−718.

(20) Norrish, K.; Hutton, J. T. An Accurate X-Ray Spectrographic Method for The Analysis of a Wide Range of Geological Samples. *Geochim. Cosmochim. Acta* **1969**, *33*, 431−453.

(21) Speakman, S. A. Introduction to PANalytical X'Pert HighScore Plus v3. 0. Ph.D. Thesis, MIT Center for Materials Science and Engineering, 2012, pp 1−19.

(22) Rietveld, H. M. A Profile Refinement Method for Nuclear and Magnetic Structures. *J. Appl. Crystallogr.* **1969**, *2*, 65−71.

(23) Okolo, G. N.; Everson, R. C.; Neomagus, H. W. J. P.; Roberts, M. J.; Sakurovs, R. Comparing the Porosity and Surface Areas of Coal as Measured by Gas Adsorption, Mercury Intrusion and SAXS Techniques. *Fuel* **2015**, *141*, 293−304.

(24) Mphahlele, K.; Matjie, R. H.; Osifo, P. O. Thermodynamics, kinetics and thermal decomposition characteristics of sewage sludge during slow pyrolysis. *J. Environ. Manage.* **2021**, *284*, 112006.

(25) Starink, M. J. A New Method for the Derivation of Activation Energies from Experiments Performed at Constant Heating Rate. *Thermochim. Acta* **1996**, *288*, 97−104.

(26) Moyo, A.; Filho, J. A.; Harrison, S.; Broadhurst, J. Characterising the Environmental Risks of Coal Preparation Wastes: A Study of Ne Coal Slurry Waste and Discards from South African Collieries. *The 11th ICARD|IMWA|MWD Conference—"Risk to Opportunity"*; International Mine Water Association, 2018; pp 417−423.

(27) Matjie, R.; Bunt, J.; Stokes, W.; Bijzet, H.; Mphahlele, K.; Uwaoma, R.; Strydom, C. Interactions Between Kaolinite, Organic Matter, and Potassium Compounds at Elevated Temperatures During Pyrolysis of Caking Coal and Its Density-Separated Fractions. *Energy Fuels* **2021**, *35*, 13268−13280.

(28) Mphahlele, K.; Matjie, R. H.; Bunt, J. R.; Uwaoma, R. C. Properties and Reactivity of Two Oxidized and Unoxidized South African Highveld Fine Coal Rejects and Their Density-Separated Fractions. *Int. J. Coal Prep. Util.* **2023**, *43* (8), 1451−1477.

(29) Wagner, N. J.; Hlatshwayo, B. The occurrence of potentially hazardous trace elements in five Highveld coals, South Africa. *Int. J. Coal Geol.* **2005**, *63*, 228−246.

(30) Hower, J. C.; Dai, S.; Seredin, V. V.; Zhao, L.; Kostova, I. J.; Silva, L. F. O.; Mardon, S. M.; Gurdal, G. A Note on the Occurrence of Yttrium and Rare Earth Elements in Coal Combustion Products. *Coal Combust. Gasif. Prod.* **2013**, *5*, 39−47.

(31) Uwaoma, R. C.; Strydom, C. A.; Matjie, R. H.; Bunt, J. R. Influence of Density Separation of Selected South African Coal Fines on the Products Obtained During Liquefaction Using Tetralin as a Solvent. *Energy Fuels* **2019**, *33*, 1837−1849.

(32) Matjie, R. H.; Lesufi, J. M.; Bunt, J. R.; Strydom, C. A.; Schobert, H. H.; Uwaoma, R. In situ Capturing and Absorption of Sulfur Gases Formed During Thermal Treatment of South African Coals. *ACS Omega* **2018**, *3*, 14201−14212.

(33) Du, Z.; Li, W. The Catalytic Effect from Alkaline Elements on the Tar-Rich Coal Pyrolysis. *Catalysts* **2022**, *12*, 376.

(34) Everson, R. C.; Neomagus, H. W. J. P.; Kasaini, H.; Njapha, D. Reaction kinetics of pulverized coal-chars derived from inertinite-rich coal discards: Characterisation and combustion. *Fuel* **2006**, *85*, 1067−1075.

(35) Shivakumara, S.; Penki, T. R.; Munichandraiah, N. High Specific Surface Area α-Fe$_2$O$_3$ Nanostructures as High Performance Electrode Material for Supercapacitors. *Mater. Lett.* **2014**, *131*, 100−103.

(36) Dai, S.; Zou, J.; Jiang, Y.; Ward, C. R.; Wang, X.; Li, T.; Xue, W.; Liu, S.; Tian, H.; Sun, X.; Zhou, D. Mineralogical and

Geochemical Compositions of The Pennsylvanian Coal in The Adaohai Mine, Daqingshan Coalfield, Inner Mongolia, China: Modes of Occurrence and Origin of Diaspore, Gorceixite, and Ammonian Illite. *Int. J. Coal Geol.* **2012**, *94*, 250−270.

(37) Ahmad, T.; Awan, I. A.; Nisar, J.; Ahmad, I. Influence of Inherent Minerals and Pyrolysis Temperature on The Yield of Pyrolysates of Some Pakistani Coals. *Energy Convers. Manage.* **2009**, *50*, 1163−1171.

(38) Matjie, R. H.; Li, Z.; Ward, C. R.; Bunt, J. R.; Strydom, C. A. Determination of Mineral-Matter and Elemental Composition of Individual Macerals in Coals from Highveld Mines. *J. South. Afr. Inst. Min. Metall.* **2016**, *116*, 169−180.

(39) Binnewies, M.; Milke, E. *Thermochemical Data of Elements and Compounds*, 2nd ed.; Wiley VCH: Weinheim, 2002; Vol. *168*.

(40) Liu, L.; Yuan, Y.; Kumar, S.; Wang, Z.; He, Y.; Lv, Y.; Liu, J.; Gul-e-Rana, J.; Cen, K. Catalytic Effect of Metal Chlorides on Coal Pyrolysis and Gasification Part II: Effects of Acid Washing on Coal Characteristics. *Thermochim. Acta* **2018**, *666*, 41−50.

(41) Hamel, S.; Hasselbach, H.; Weil, S.; Krumm, W. Autothermal Two-Stage Gasification of Low-Density Waste-Derived Fuels. *Energy* **2007**, *32*, 95−107.

(42) Ban, Y.; Jin, L.; Zhu, J.; Liu, F.; Hu, H. Insights into Effect of $Ca(OH)_2$ on Pyrolysis Behaviors and Products Distribution of Hongshaquan Coal. *Fuel* **2022**, *307*, 121791.

(43) Le, J.; Liu, P.; Liu, D.; Lu, X.; Pan, T.; Zhang, D. Effect of Catalysts on the Yields of Light Components and Phenols Derived from Shenmu Coal Low Temperature Pyrolysis. *Energy Fuels* **2017**, *31*, 7033−7041.

(44) Shi, Z.; Jin, L.; Zhou, Y.; Li, H.; Li, Y.; Hu, H. In-situ Analysis of Catalytic Pyrolysis of Baiyinhua Coal with Pyrolysis Time-of-Flight Mass Spectrometry. *Fuel* **2018**, *227*, 386−393.

(45) Zheng, M.; Li, X.; Nie, F.; Guo, L. Investigation of Overall Pyrolysis Stages for Liulin Bituminous Coal by Large-Scale ReaxFF Molecular Dynamics. *Energy Fuels* **2017**, *31*, 3675−3683.

(46) Shi, Z.; Jin, L.; Zhou, Y.; Li, Y.; Hu, H. Online Analysis of Initial Volatile Products of Shenhua Coal and its Macerals with Pyrolysis Vacuum Ultraviolet Photoionization Mass Spectrometry. *Fuel Process. Technol.* **2017**, *163*, 67−74.

(47) Shao, S.; Ma, B.; Wang, C.; Chen, Y. Thermal Behavior and Chemical Reactivity of Coal Gangue During Pyrolysis and Combustion. *Fuel* **2023**, *331*, 125927.

(48) Shi, X.; Wu, Y.; Zhang, J.; Ding, L.; Wang, C.; Lan, X.; Gao, J. Comparison of Pyrolysis Behavior Between Pure Coal and Mixture of Coal/CaO. *J. Anal. Appl. Pyrolysis* **2021**, *159*, 105311.